Visual Abstract

Free vibration analysis of porous functionally graded plates using a novel Quasi-3D hyperbolic high order shear deformation theory

Mohammed Amine Kenanda
ENERGARID Laboratory, Department of Mechanical Engineering, Tahri Mohamed University, 08000 Bechar, Algeria
kenandaamine@gmail.com or kenanda.mohammedamine@univ-bechar.dz

Fodil Hammadi
Laboratory of Mechanics, Modeling and Experimentation L2ME, Department of Mechanical Engineering, Tahri Mohamed University, 08000 Bechar, Algeria
hammadi.fodil@univ-bechar.dz

Zakaria Belabed
Department of Technology, Institute of Science and Technology, University Ctr Naama, 45000 Naama, Algeria
belabed.zak@gmail.com

Mohammed Hadj Meliani
LPTPM, Hassiba BenBouali University of Chlef, 02000, Chlef, Algeria
m.hadjmeliani@univ-chlef.dz

ABSTRACT. In this study, a novel quasi-three dimensional hyperbolic high-order shear deformation theory (quasi-3D HHSDT) is developed for free vibration analysis of porous functionally graded plates (FGPs). There are six unknowns in the current displacement field, and no shear correction factor is required. The mechanical properties are varied continuously through the thickness of porous FG plates using a modified power law function while considering the effect of porosities on the plate's structural integrity. Two distinct porosity distribution models are considered, including even and uneven porosity distributions. The Navier technique is employed to obtain the closed-form solutions of motion's equations. An exhaustive parametric study is presented to show the influence of the different parameters on the fundamental frequencies.

KEYWORDS. High-order shear deformation theory, Porous FG plate, Free vibration.

OPEN ACCESS

Citation: Kenanda, M. A., Hammadi, F., Belabed, Z., Meliani, M.H., Free vibration analysis of porous functionally graded plates using a novel Quasi-3D hyperbolic high order shear deformation theory, Frattura ed Integrità Strutturale, 64 (2023) 266-282.

Received: 30.01.2023
Accepted: 16.03.2023
Online first: 21.03.2023
Published: 01.04.2023

INTRODUCTION

Functionally graded materials (FGMs) are a novel type of composite material, characterized by a gradual and continuous variation in the volume fractions of each of their constituents (generally metal and ceramic) throughout their thickness. A team of Japanese researchers has developed FGMs for use in the space industry due to their exceptional properties and advantages, such as high-temperature resistance, corrosion resistance, and oxidation resistance, among others.

Numerous studies are conducted on mechanical behavior (i.e., buckling, bending, and free vibration analysis) based on high-order shear deformation theories, including third-order, exponential, sinusoidal, etc. Reddy et al. [1–3] used third-order shear deformation theory to study the mechanical behavior of isotropic and FG plates and beams. Following that, several research projects have been carried out in order to develop new theories based on Reddy's theory (e.g., hyperbolic-trigonometric [4–13], trigonometric [14–18], exponential [19], trigonometric-exponential [20], exponential-logarithmic [21], and polynomial [22–25]). Li et al [26–28] studied static and free vibration behavior of FG plates employing novel polynomial theories with shape parameter (m). Hadji et al. [29] studied the effect of porosities and Winkler-Pasternak parameters on the bending of porous FG sandwich plates using quasi-3D sinusoidal shear deformation theory. They condensed the number of variables into only five by employing a displacement field with integral-undefined terms. Boulefrakh et al. [30] employed a simple hyperbolic shear deformation theory to study the effect of visco-Pasternak parameters on the mechanical behavior of thick FG plates. They included the stretching effect with only four variables compared to the previous displacement fields, which had many variables. Based on isogeometric analysis, Cuong-Le et al. [31] conducted a 3D numerical solution for the mechanical behavior of porous FG annular plates, cylindrical shells, and conical shells using a NURBS basic function. According to the findings, the quadratic NURBS element can produce high-accuracy results with the least amount of computational cost. Cuong-Le et al. [32] used a nonlocal strain gradient, Reissner-Mindlin plate theory, and isogeometric analysis for the bending, buckling, and free vibration of sigmoid FG nanoplates. Vu et al. [33] developed a new refined quasi-3D hyperbolic shear deformation theory combined with the Navier solution to analyze the compressive buckling of porous FG plates placed on the Winkler-Pasternak foundation.

Based on the moving kriging interpolation meshfree method and a novel arctangent exponential shear deformation theory, Vu et al. [34] presented a mechanical behavior analysis of sandwich FG plates. They used a displacement field with only four unknowns. Two models of refined high-order theories (inverse sin and sin hyperbolic shear deformation) were developed by Vu et al. [35, 36] to analyze the bending, buckling, and free vibration behavior of FG plates by employing the enhanced meshfree method with new correlation functions. Vu et al. [37] and Tan-Van Vu [38] conducted a mechanical behavior analysis of an FG plate resting on elastic foundations based on a refined quasi-3D logarithmic shear deformation theory and a simple quasi-3D hyperbolic shear deformation theory, respectively. The new refined high-order theories mentioned in the references [33–38], which were combined with the meshfree method, showed many advantages, including the mathematical simplicity of their modeling, the lowest computational cost, and the accuracy compared to many high-order shear deformation theories.

Due to technical issues, porosities may appear inside the material during FGM manufacturing. Porosities can significantly affect the mechanical properties and lower the FGM strength [39]. Farzad Ebrahimi and Ali Jafari [40] employed two distributions of porosities (even and uneven distributions) to study the influence of porosities on the thermo-mechanical vibration of FG beams. Yan Qing Wang [41] investigated the electro-mechanical behavior of porous FG piezoelectric plates in translation using an even porosity distribution. Based on four symmetric and asymmetric distributions of porosities, Tao et al. [42] analyzed the thermo-acoustic response of a porous FG cylindrical shell bounded by the Pasternak foundation under nonlinear thermal loading using the first-order shear deformation theory. Saidi Hayat and Sahla Meriem [43] developed a novel distribution of porosities (as an exponential function) to analyze the free vibration of porous FG plates made of a mixture of aluminum (Al) and alumina (Al_2O_3) resting on an elastic foundation. Thanh et al. [44] used a logarithmic-uneven distribution of porosities and isogeometric analysis to study the thermal stability of porous FG microplates.

In this context and to enhance concepts about high-order shear deformation theories and the FG plate's structural integrity, a novel quasi-three-dimensional hyperbolic high-order shear deformation theory (quasi-3D HHSDT) is developed to study the free vibration behavior of porous FG plates using two distinct porosity distribution models (even and linear-uneven distribution). The proposed hyperbolic theory is more affluent and presents the transverse shear stress better than third-order, sinusoidal, and exponential shear deformation theories and thus produces better results in describing the mechanical behavior of FG plates. Moreover, the current hyperbolic function does not necessitate a shear

correction factor and does not require any adaptation in the event that it is employed as a refined theory. This is due to its form, which is partitioned into two segments, similar to the third-order shear deformation theory.
The article has been organized as follows: First, the material properties of porous FG plate based on a power-law function (P-FGM) are presented in section 2. The displacement field and strain, the constitutive law, and equations of motion are introduced in section 3. The analytical solution for simply supported plate in bending and free vibration by using Navier's solution approach is illustrated in section 4. Section 5 presents numerical results, a comparative study, and the effects of various parameters (power-law index, geometrical ratio, etc.). In section 6, the conclusion and major results are described.

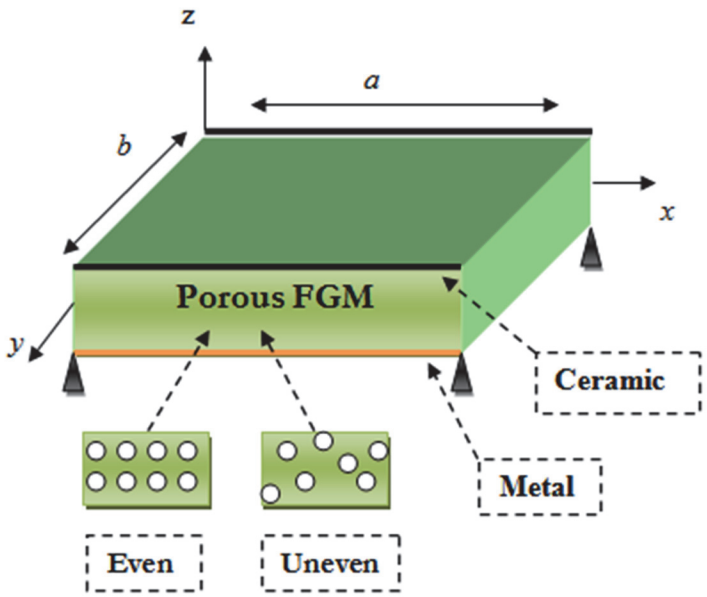

Figure 1: Geometry and coordinates of porous functionally graded plate.

MATERIAL PROPERTIES OF POROUS FG PLATE

A rectangular porous plate of length (a), width (b), and thickness (h), made of functionally graded material (FGM), where the top surface of the FG plate is made of ceramic and the bottom surface of metal, as shown in Fig. 1. The material properties of porous FG plate are based on a power-law function (P-FGM) as follows:

- Perfect FGM:

$$\eta(z)=\eta_m+(\eta_c-\eta_m)\left(\frac{z}{h}+\frac{1}{2}\right)^P \tag{1a}$$

- Porous FGM (even distribution):

$$\eta(z)=\eta_m+(\eta_c-\eta_m)\left(\frac{z}{h}+\frac{1}{2}\right)^P-\frac{\beta}{2}(\eta_c+\eta_m) \tag{1b}$$

- Porous FGM (uneven distribution):

$$\eta(z)=\eta_m+(\eta_c-\eta_m)\left(\frac{z}{h}+\frac{1}{2}\right)^P-\frac{\beta}{2}(\eta_c+\eta_m)\left(1-\frac{2|z|}{h}\right) \tag{1c}$$

In which

$$0 \le \beta \le 1 \tag{1d}$$

where (η) denotes the material properties, including the elastic modulus E, mass density ρ, and Poisson's ratio ν. P and β are the power law and porosity parameters, respectively.

THEORY AND FORMULATION

According to high-order shear deformation theory, including the thickness stretching effect, the displacement field can be described as:

$$\begin{Bmatrix} u(x,y,z,t) \\ v(x,y,z,t) \\ w(x,y,z,t) \end{Bmatrix} = \begin{Bmatrix} u_0(x,y,t) - z\dfrac{\partial w_0}{\partial x} + f(z)\theta_x(x,y,t) \\ v_0(x,y,t) - z\dfrac{\partial w_0}{\partial y} + f(z)\theta_y(x,y,t) \\ w_0(x,y,t) + g(z)\theta_z(x,y,t) \end{Bmatrix} \tag{2}$$

In which

$$g(z) = \frac{d f(z)}{d z}$$

In which t signifies the time, (x, y, z) are the Cartesian coordinates, u_0, v_0, w_0, θ_x, θ_y and θ_z are the mid-plane displacement and rotation components along the x, y and z directions, respectively, $f(z)$ is a shape function for describing the distribution of transverse shear stress. The most famous theories of high-order shear deformation are presented in Tab. 1 and Fig. 2.

Theories	$f(z)$	Authors
Third-order shear deformation theory	$z - \frac{4z^3}{3h^2}$	Reddy [1]
Trigonometric high-order shear deformation theory	$\frac{h}{\pi}\sin\left(\frac{\pi z}{h}\right)$	Touratier [14]
Exponential high-order shear deformation theory	$z\exp\left(-2\left(\frac{z}{h}\right)^2\right)$	Karama et al.[19]
arctangent exponential high-order shear deformation theory	$\tan^{-1}\left(z\exp\left(-2\left(\frac{z}{h}\right)^2\right)\right)$	Vu et al. [34]
Hyperbolic high-order shear deformation theory	$-\frac{R\,h\tanh\left(\frac{z}{h}\right)\left(\tanh^2\left(\frac{z}{h}\right)-3\right)}{3\operatorname{sech}^4(0.5)} - R\,z; \quad R = 1.62$	Present

Table 1: The most famous high-order shear deformation theories.

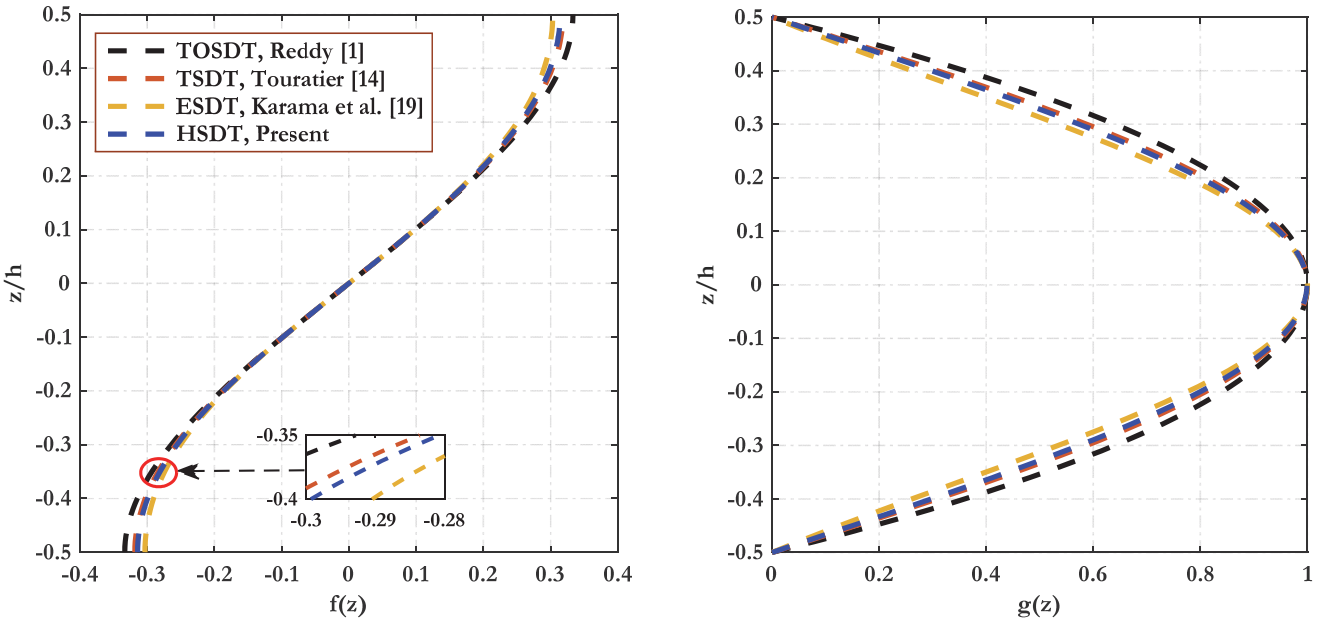

Figure 2: The variation of the shape functions $f(z)$ and its derivative $g(z)$ in terms of non-dimensional thickness (z/h).

The new shear deformation function is developed based on the following conditions:

$$\int_{z=-\frac{h}{2}}^{z=+\frac{h}{2}} f(z)\,dz = 0 \quad ; \quad g(z)\big|_{z=\pm\frac{h}{2}} = 0 \quad ; \quad g(z)\big|_{z=0} = 1 \tag{3}$$

The linear strain field of a porous FG plate can be deduced from the displacement field in Eqn. (2) as:

$$\begin{Bmatrix} \varepsilon_x \\ \varepsilon_y \\ \varepsilon_z \end{Bmatrix} = \begin{Bmatrix} \dfrac{\partial u_0}{\partial x} - z\dfrac{\partial^2 w_0}{\partial x^2} + f(z)\dfrac{\partial \theta_x}{\partial x} \\ \dfrac{\partial v_0}{\partial y} - z\dfrac{\partial^2 w_0}{\partial y^2} + f(z)\dfrac{\partial \theta_y}{\partial y} \\ g'(z)\theta_z(x,y,t) \end{Bmatrix} \tag{4a}$$

$$\begin{Bmatrix} \gamma_{xy} \\ \gamma_{yz} \\ \gamma_{xz} \end{Bmatrix} = \begin{Bmatrix} \dfrac{\partial u_0}{\partial y} + \dfrac{\partial v_0}{\partial x} - 2z\dfrac{\partial^2 w_0}{\partial x \partial y} + f(z)\left(\dfrac{\partial \theta_x}{\partial y} + \dfrac{\partial \theta_y}{\partial x}\right) \\ g(z)\left(\theta_y + \dfrac{\partial \theta_z}{\partial y}\right) \\ g(z)\left(\theta_x + \dfrac{\partial \theta_z}{\partial x}\right) \end{Bmatrix} \tag{4b}$$

The constitutive law is characterized by the relationship between the stress field and the strain field (Hook's law), as:

$$\begin{Bmatrix}\sigma_x\\ \sigma_y\\ \sigma_z\\ \tau_{yz}\\ \tau_{xz}\\ \tau_{xy}\end{Bmatrix}=\begin{bmatrix}C_{11} & C_{12} & C_{13} & 0 & 0 & 0\\ C_{12} & C_{22} & C_{23} & 0 & 0 & 0\\ C_{13} & C_{23} & C_{33} & 0 & 0 & 0\\ 0 & 0 & 0 & C_{44} & 0 & 0\\ 0 & 0 & 0 & 0 & C_{55} & 0\\ 0 & 0 & 0 & 0 & 0 & C_{66}\end{bmatrix}\begin{Bmatrix}\varepsilon_x\\ \varepsilon_y\\ \varepsilon_z\\ \gamma_{yz}\\ \gamma_{xz}\\ \gamma_{xy}\end{Bmatrix} \tag{5}$$

where $(\sigma_x,\sigma_y,\sigma_z,\tau_{yz},\tau_{xz},\tau_{xy})$ and $(\varepsilon_x,\varepsilon_y,\varepsilon_z,\gamma_{yz},\gamma_{xz},\gamma_{xy})$ are the stress and strain components, respectively, C_{ij} indicating the stiffness coefficients are defined as:

$$\begin{cases}C_{11}=C_{22}=C_{33}=\dfrac{E(z)(1-\nu)}{(1-2\nu)(1+\nu)}\\ C_{12}=C_{13}=C_{23}=\dfrac{\nu E(z)}{(1-2\nu)(1+\nu)}\\ C_{44}=C_{55}=C_{66}=G(z)=\dfrac{E(z)}{2(1+\nu)}\end{cases} \tag{6}$$

where ν represents Poisson's ratio, E(z) and G(z) are the Young's and shear modulus of the porous FG plate, respectively.

EQUATIONS OF MOTION

Based on Hamilton's principle, the equations of motion can be expressed by the following variation form:

$$\int_0^t\left(\delta E_s+\delta E_p-\delta E_k\right)dt=0 \tag{7}$$

where δ represents the variation operator, $\delta E_s,\delta E_p$, and δE_k are the variation of strain energy, the variation of the potential energy due to the applied loads, and the variation of kinetic energy, respectively. The variation of strain energy of the porous FG plate takes the form below:

$$\delta E_s=\int_V\left[\sigma_x\,\delta\varepsilon_x+\sigma_y\,\delta\varepsilon_y+\sigma_z\,\delta\varepsilon_z+\tau_{xy}\,\delta\gamma_{xy}+\tau_{yz}\,\delta\gamma_{yz}+\tau_{xz}\,\delta\gamma_{xz}\right]dV \tag{8}$$

The variation of potential energy due to the applied loads is given by:

$$\delta E_p=-\int_A\left(q\,\delta w\right)dA \tag{9}$$

in which q represents the transverse distributed load, A is the top surface. The variation of kinetic energy of the porous FG plate is deduced by the following integral as:

$$\delta E_k=\int_V\left[\frac{\partial u}{\partial t}\frac{\partial\delta u}{\partial t}+\frac{\partial v}{\partial t}\frac{\partial\delta v}{\partial t}+\frac{\partial w}{\partial t}\frac{\partial\delta w}{\partial t}\right]\rho(z)\,dV \tag{10}$$

Eqns. (8), (9), and (10) are substituted into Eqn. (7), and the linear strain field expressions (4a, 4b), and constitutive law expressions (5) are used in Eqn. (7). The equations of motion are obtained as:

$$\delta u_0 : \frac{\partial N_x}{\partial x}+\frac{\partial N_{xy}}{\partial y}=D_1\frac{\partial^2 u_0}{\partial t^2}-D_2\frac{\partial^3 w_0}{\partial t^2\partial x}+D_4\frac{\partial^2 \theta_x}{\partial t^2}$$

$$\delta v_0 : \frac{\partial N_{xy}}{\partial x}+\frac{\partial N_y}{\partial y}=D_1\frac{\partial^2 v_0}{\partial t^2}-D_2\frac{\partial^3 w_0}{\partial t^2\partial y}+D_4\frac{\partial^2 \theta_y}{\partial t^2}$$

$$\delta w_0 : \frac{\partial^2 M_x}{\partial x^2}+2\frac{\partial^2 M_{xy}}{\partial x\partial y}+\frac{\partial^2 M_y}{\partial y^2}=D_1\frac{\partial^2 w_0}{\partial t^2}+D_2\left(\frac{\partial^3 u_0}{\partial t^2\partial x}+\frac{\partial^3 v_0}{\partial t^2\partial y}\right)$$
$$-D_3\left(\frac{\partial^4 w_0}{\partial t^2\partial x^2}+\frac{\partial^4 w_0}{\partial t^2\partial y^2}\right)+D_5\left(\frac{\partial^3 \theta_x}{\partial t^2\partial x}+\frac{\partial^3 \theta_y}{\partial t^2\partial y}\right)+D_7\frac{\partial^2 \theta_z}{\partial t^2} \quad (11)$$

$$\delta\theta_x : \frac{\partial S_x}{\partial x}+\frac{\partial S_{xy}}{\partial y}-Q_{xz}=D_4\frac{\partial^2 u_0}{\partial t^2}-D_5\frac{\partial^3 w_0}{\partial t^2\partial x}+D_6\frac{\partial^2 \theta_x}{\partial t^2}$$

$$\delta\theta_y : \frac{\partial S_{xy}}{\partial x}+\frac{\partial S_y}{\partial y}-Q_{yz}=D_4\frac{\partial^2 v_0}{\partial t^2}-D_5\frac{\partial^3 w_0}{\partial t^2\partial y}+D_6\frac{\partial^2 \theta_y}{\partial t^2}$$

$$\delta\theta_z : \frac{\partial Q_{xz}}{\partial x}+\frac{\partial Q_{yz}}{\partial y}-N_z=D_7\frac{\partial^2 w_0}{\partial t^2}+D_8\frac{\partial^2 \theta_z}{\partial t^2}$$

where the moment, the stress resultants (N_{ij}, M_{ij}, S_{ij} and Q_{ij}), and the moments of inertia (D_{ij}) are defined in Appendix A.

ANALYTICAL SOLUTION

According to Navier's solution approach for simply supported FG plate, the analytical solutions of motion's Eqns. (11) are expanded relying on double Fourier series:

$$\begin{Bmatrix} u_0(x,y)\\ v_0(x,y)\\ w_0(x,y)\\ \theta_x(x,y)\\ \theta_y(x,y)\\ \theta_z(x,y)\end{Bmatrix}=\sum_{m=1}^{\infty}\sum_{n=1}^{\infty}\begin{Bmatrix} U_{mn}\cos(\lambda x)\sin(\mu y)e^{i\omega t}\\ V_{mn}\sin(\lambda x)\cos(\mu y)e^{i\omega t}\\ W_{mn}\sin(\lambda x)\sin(\mu y)e^{i\omega t}\\ \phi^x_{mn}\cos(\lambda x)\sin(\mu y)e^{i\omega t}\\ \phi^y_{mn}\sin(\lambda x)\cos(\mu y)e^{i\omega t}\\ \phi^z_{mn}\sin(\lambda x)\sin(\mu y)e^{i\omega t}\end{Bmatrix} \quad (12a)$$

in which

$$\lambda=m\pi/a \quad ; \quad \mu=n\pi/b \quad (12b)$$

where ω is the natural frequency, (m, n) are the frequency mode numbers, U_{mn}, V_{mn}, W_{mn}, ϕ^x_{mn}, ϕ^y_{mn} and ϕ^z_{mn} are coefficients must be determined. According to the Eqns. (11 and 12), the eigenvalue problem can be expressed in algebraic form as:

$$\left([S]_{ij}-\omega^2[m]_{ij}\right)\{\Delta\}_j=\{0\}_j \qquad (i,j=1,6) \quad (13a)$$

in which

$$\{\Delta\}^{T} = \left\{U_{mn}, V_{mn}, W_{mn}, \phi^{x}_{mn}, \phi^{y}_{mn}, \phi^{z}_{mn}\right\} \tag{13b}$$

The coefficients of matrices [S] and [m] can be deduced as:

$$\begin{aligned}
&S_{11} = -A_{11}\lambda^2 - A_{33}\mu^2, && S_{12} = -\lambda\mu\left(A_{12} + A_{33}\right)\\
&S_{13} = B_{11}\lambda^3 + \lambda\mu^2\left(B_{12} + 2B_{33}\right), && S_{14} = -V_{11}\lambda^2 - V_{33}\mu^2\\
&S_{15} = -\lambda\mu\left(V_{12} + V_{33}\right), && S_{16} = D_{11}\lambda\\
&S_{22} = -A_{33}\lambda^2 - A_{22}\mu^2, && S_{23} = B_{22}\mu^3 + \lambda^2\mu\left(B_{12} + 2B_{33}\right)\\
&S_{24} = -\lambda\mu\left(V_{12} + V_{33}\right), && S_{25} = -V_{33}\lambda^2 - V_{22}\mu^2\\
&S_{26} = D_{12}\mu, && S_{33} = -E_{11}\lambda^4 - \lambda^2\mu^2\left(2E_{12} + 4E_{33}\right) - E_{22}\mu^4\\
&S_{34} = F_{11}\lambda^3 + \lambda\mu^2\left(F_{12} + 2F_{33}\right), && S_{35} = F_{22}\mu^3 + \lambda^2\mu\left(F_{12} + 2F_{33}\right)\\
&S_{36} = -G_{11}\lambda^2 - G_{12}\mu^2, && S_{44} = -M_{44} - H_{11}\lambda^2 - H_{33}\mu^2\\
&S_{45} = -\lambda\mu\left(H_{12} + H_{33}\right), && S_{46} = \lambda\left(K_{11} - M_{44}\right)\\
&S_{55} = -M_{55} - H_{33}\lambda^2 - H_{22}\mu^2, && S_{56} = \mu\left(K_{12} - M_{55}\right)\\
&S_{66} = -L_{11} - M_{44}\lambda^7 - M_{55}\mu^2
\end{aligned} \tag{14a}$$

$$\begin{aligned}
&m_{11} = m_{22} = D_1, && m_{13} = -\lambda D_2, && m_{14} = m_{25} = D_4, && m_{23} = -\mu D_2\\
&m_{33} = D_1 + D_3\left(\lambda^2 + \mu^2\right), && m_{34} = -\lambda D_5, && m_{35} = -\mu D_5 &&\\
&m_{36} = D_7, && m_{44} = m_{55} = D_6, && m_{66} = D_8 &&\\
&m_{12} = m_{15} = m_{16} = m_{24} = m_{26} = m_{46} = m_{45} = m_{56} = 0 &&&&&&
\end{aligned} \tag{14b}$$

where the stiffness coefficients $(A_{ij}, B_{ij}, V_{ij}, D_{ij}, E_{ij}, F_{ij}, G_{ij}, K_{ij}, L_{ij})$ are indicated in Appendix B.

RESULTS AND DISCUSSION

From the previous theoretical development, this section examines the competence and accuracy of the above-mentioned theory (see Tab. 1) in comparison with popular benchmark linear analysis. This part is divided into four basic examples for confirming the correctness and effectiveness of the current theory and for studying, in particular, the influence of certain parameters such as the power-law index and the effect of geometric and material properties (the effect of the (a/b) and (a/h) ratios, etc.).The material properties and non-dimensional parameters are defined as follows:

- Material properties:

The properties of aluminum (AL) are: $E_m = 70\,GPa$; $\rho_m = 2702\,kg/m^3$; $\nu_m = 0.3$

The properties of alumina (AL_2O_3) are: $E_c = 380\,GPa$; $\rho_c = 3800\,kg/m^3$; $\nu_c = 0.3$

The properties of zirconia (ZrO_2) are: $E_c = 200\,GPa$; $\rho_c = 5700\,kg/m^3$; $\nu_c = 0.3$

- Boundary conditions:

$N_x = v = w = M_x = S_x = Q_{yz} = N_z = \theta_y = \theta_z = 0 \quad$ at $\quad x = 0$

$N_y = u = w = M_y = S_y = Q_{xz} = N_z = \theta_x = \theta_z = 0 \quad$ at $\quad y = 0$

- Non-dimensional parameters:

$$\bar{\omega} = \omega h\sqrt{\frac{\rho}{G}}, \quad \hat{\omega} = \omega h\sqrt{\frac{\rho_c}{E_c}}, \quad \widehat{\omega} = \omega h\sqrt{\frac{\rho_m}{E_m}}, \quad \ddot{\omega} = \omega\frac{a^2}{h}\sqrt{\frac{\rho_m}{E_m}}$$

Example 1

To confirm the correctness of the current quasi-3D theory of free vibration, this numerical example illustrates several of the non-dimensional fundamental frequencies ($\bar{\omega}$) for an isotropic square plate (i.e., P = 0, full ceramic) with (a/h = 10, moderately thick plate) as shown in Tab. 2. The current quasi-3D results are compared with the 3D exact solution obtained by Srinivas et al. [45], the quasi-3D hyperbolic HDST solutions of Akvaci and Tanrikulu [6] and Shahsavari et al.[5], the classical plate theory solution of Mechab et al. [36]. It is obvious from Tab. 2 that the present quasi-3D findings are in excellent accordance with the solutions synthesized by the references [45], [6], [5], [46]. The smallest percentage of the average difference is related to the Shahsavari's theory [5] and the maximal percentage of the average difference is related to the classical plate theory solution proposed in [46], due to the absence of the shear effect. It can also be observed from Tab. 2 that the non-dimensional fundamental frequencies increase whenever the frequency mode numbers (m, n) increase. The difference percent is counted by the formula as follows:

$$Diff\,(\%) = \left| \frac{\text{result obtained by our model}}{\text{result obtained by refrence model}} - 1 \right| \times 100$$

m	n	Ref.[45]	Ref.[6]	Ref.[5]	Ref.[46]	Present
		E-3D	Q-3D	Q-3D	CBT-2D	Q-3D
1	1	0.0932	0.0932	0.0932	0.0955	0.0934
1	2	0.2226	0.2227	0.2226	-	0.2233
2	2	0.3421	0.3424	0.3421	0.3732	0.3432
1	3	0.4171	0.4176	-	0.4629	0.4186
2	3	0.5239	0.5247	0.5240	0.5951	0.5259
3	3	0.6889	0.6902	0.6892	-	0.6919
2	4	0.7511	0.7526	0.7514	0.8926	0.7545
1	5	0.9268	0.9290	0.9274	1.1365	0.9315
Average diff. %		-	**0.130**	**0.024**	**12.932**	**0.373**

Table 2: The first eight non-dimensional fundamental frequencies ($\bar{\omega}$) of the isotropic square plate with ($a/h = 10, \varepsilon_z \neq 0$).

Example 2

The second example considers the impact of the power-law index on the fundamental frequencies ($\hat{\omega}$) for (AL/AL_2O_3) square plate. Tab. 3 contains the first three non-dimensional fundamental frequencies ($\hat{\omega}$) for moderately thick FG plate and different power-law indexes P = 0, P = 0.5, P = 1, P = 4, and P = 10. The outcomes indicated from Tab. 3 correlate supremely well with the FSDT of Hosseini-Hashemi et al. [47] and the HSDT of Belabed et al. [48]. Furthermore, when the stretching effect is removed, the current outcomes are nearly identical. Moreover, the fundamental frequencies ($\hat{\omega}$) reduce as the power-law indexes (P) increase. This is due to the influence of Young's modulus and mass density, which are high for ceramic compared to metal. In other words, the increase in the parameter (P) decreases the stiffness of the FG plate.

m	n	Theories	ε_z	power-law index (*P*)				
				0	0.5	1	4	10
1	1	FSDT [47]	= 0	0.0577	0.0490	0.0442	0.0382	0.0366
		HSDT [48]	≠ 0	0.0578	0.0494	0.0449	0.0389	0.0368
		Present	**≠ 0**	**0.0579**	**0.0495**	**0.0450**	**0.0390**	**0.0369**
1	2	FSDT [47]	= 0	0.1376	0.1173	0.1059	0.0911	0.0867
		HSDT [48]	≠ 0	0.1381	0.1184	0.1077	0.0923	0.0868
		Present	**≠ 0**	**0.1385**	**0.1187**	**0.1079**	**0.0925**	**0.0869**
2	2	FSDT [47]	= 0	0.2112	0.1805	0.1631	0.1397	0.1324
		HSDT [48]	≠ 0	0.2121	0.1825	0.1659	0.1409	0.1318
		Present	**≠ 0**	**0.2128**	**0.1830**	**0.1664**	**0.1412**	**0.1320**

Table 3: The first three non-dimensional fundamental frequencies ($\hat{\omega}$) of the (AL/AL_2O_3) square plate for several values of the power-law index with (a/h = 10).

Example 3

To consider the influence of the ratios (a/b) and (a/h) on the fundamental frequencies ($\bar{\omega}$). This numerical example depicts the non-dimensional fundamental frequencies ($\bar{\omega}$) of square and rectangle FG plates for various values of the power-law index, the ratios (a/b) and (a/h) as seen in Tab. 4. The acquired results are evaluated against high-order shear deformation theory of Zaoui et al. [20], and our results are closely related with theirs. Also, it can be seen that once the ratios (a/h) decrease, the fundamental frequencies increase. On the contrary, the fundamental frequencies decrease when the ratios (a/b) increase.

b/a	a/h	P	Ref.[20] (Q-3D)	Ref.[20] (2D)	Present (Q-3D)
1	10	0	0.1137	0.1134	0.1138
		1	0.0883	0.0868	0.0884
		2	0.0807	0.0788	0.0808
		5	0.0756	0.0740	0.0757
	5	0	0.4178	0.4151	0.4182
		1	0.3267	0.3205	0.3270
		2	0.2968	0.2892	0.2970
		5	0.2725	0.2665	0.2726
	2	0	1.8583	1.8287	1.8607
		1	1.4830	1.4467	1.4848
		2	1.3269	1.2901	1.3284
		5	1.1576	1.1310	1.1585
2	10	0	0.0719	0.0717	0.0720
		1	0.0558	0.0549	0.0559
		2	0.0511	0.0498	0.0511
		5	0.0480	0.0470	0.0480
	5	0	0.2718	0.2705	0.2720
		1	0.2119	0.2081	0.2121
		2	0.1930	0.1882	0.1932
		5	0.1788	0.1749	0.1789
	2	0	1.3086	1.2914	1.3102
		1	1.0378	1.0140	1.0389
		2	0.9322	0.9069	0.9332
		5	0.8250	0.8062	0.8255

Table 4: The non-dimensional fundamental frequencies ($\bar{\omega}$) of the (AL/AL_20_3) plate for several values of the power-law index, the ratios (a/b) and (a/h) with (m = n = 1).

Example 4

The final example examines the implications of the porosities on the fundamental frequencies ($\hat{\omega}$) and structural integrity of an (AL/AL_2O_3) square plate. The Figs. 3–4 represent the first non-dimensional fundamental frequencies (ω) of a porous (AL/AL_20_3) plate in terms of the porosity parameter β for various ratios (a/h) of 20, 10, and 5 (i.e., from thin to thick plate) at P = 1 by using two types of porosity distribution (even and uneven distributions). It can be clearly observed from the figures that the fundamental frequencies decrease for all values of ratios (a/h) as the porosity parameter β increases in the case of an even porosity distribution. On the contrary, in the case of an uneven porosity distribution, the fundamental frequencies increase as the porosity parameter β increases. The two distributions affect the frequencies in completely opposite ways due to the effect of the $\left(1-\left(\frac{2|\tilde{z}|}{h}\right)\right)$ function, which is present in one and absent in the other (see Eqns. 1b and 1c).

Upon examination of the Figs. 3 and 4 presented, it is apparent that the impact of even porosity distribution exceeds that of uneven porosity distribution. This is demonstrated by the significant decrease of fundamental frequencies in the range of [8.2, 9] across all (a/h) ratios, which culminates in the range of [5.8, 6.3] at β = 0.5. Conversely, an increase in fundamental frequencies from the range of [8.2, 9] to the range of [8.3, 9.4] is observed when the porosity parameter attains a value of 0.5. Consequently, it can be deduced that the effect of the even porosity distribution is more pronounced and substantial when compared to the uneven porosity distribution.

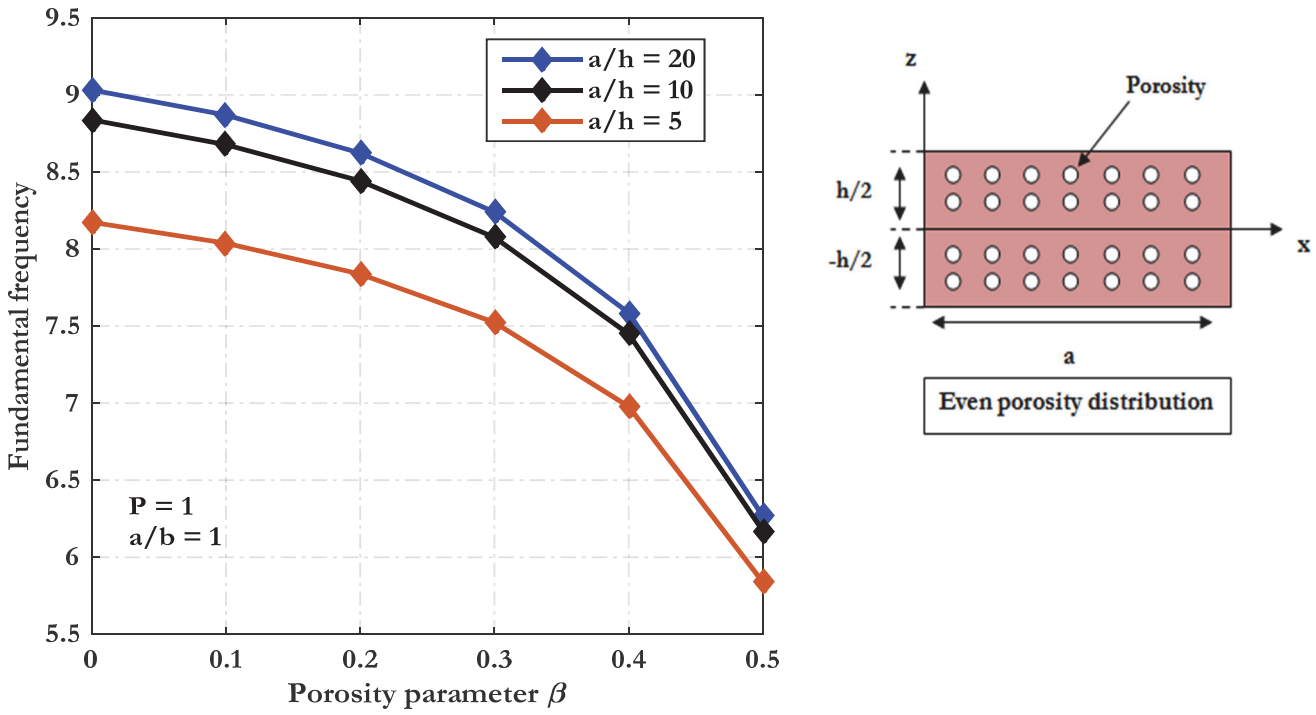

Figure 3: The non-dimensional fundamental frequencies (ω) of a porous (AL/AL_2O_3) plate in terms of the porosity parameter for various ratios (a/h), with an even porosity distribution and (m = n = 1).

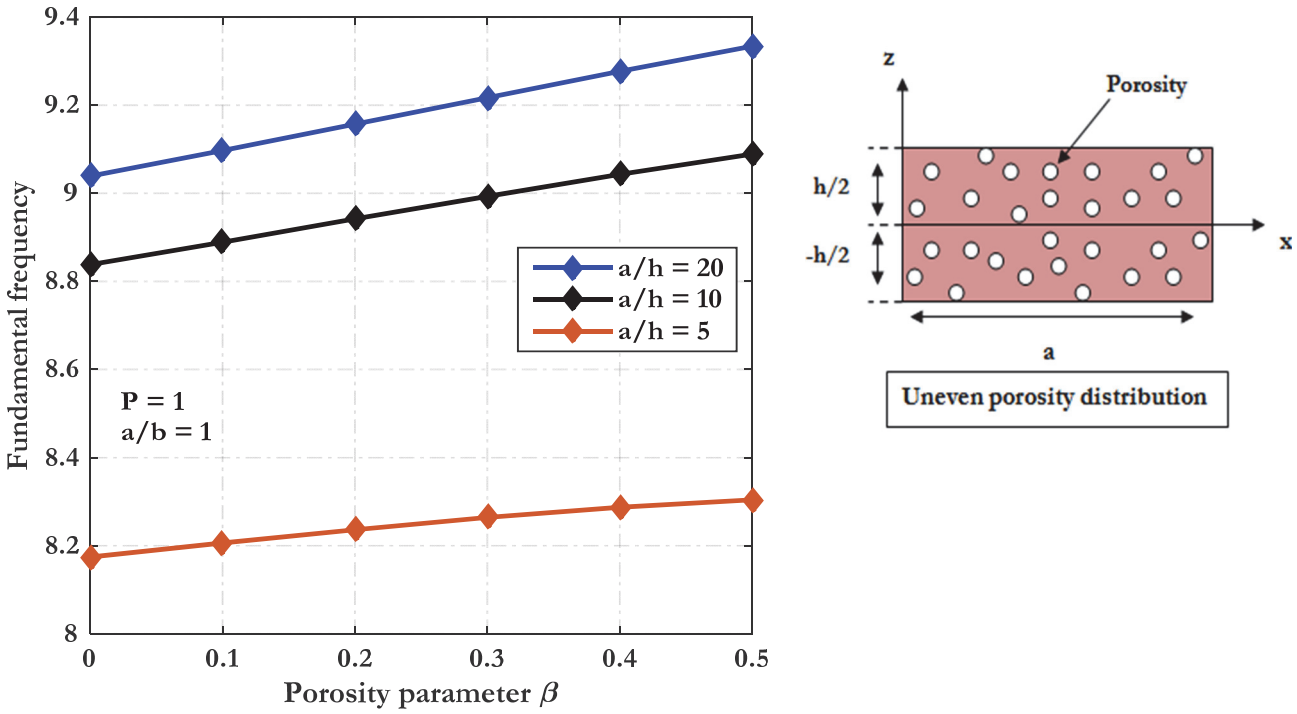

Figure 4: The non-dimensional fundamental frequencies (ω) of a porous (AL/AL_2O_3) plate in terms of the porosity parameter for various ratios (a/h), with an uneven porosity distribution and (m = n = 1).

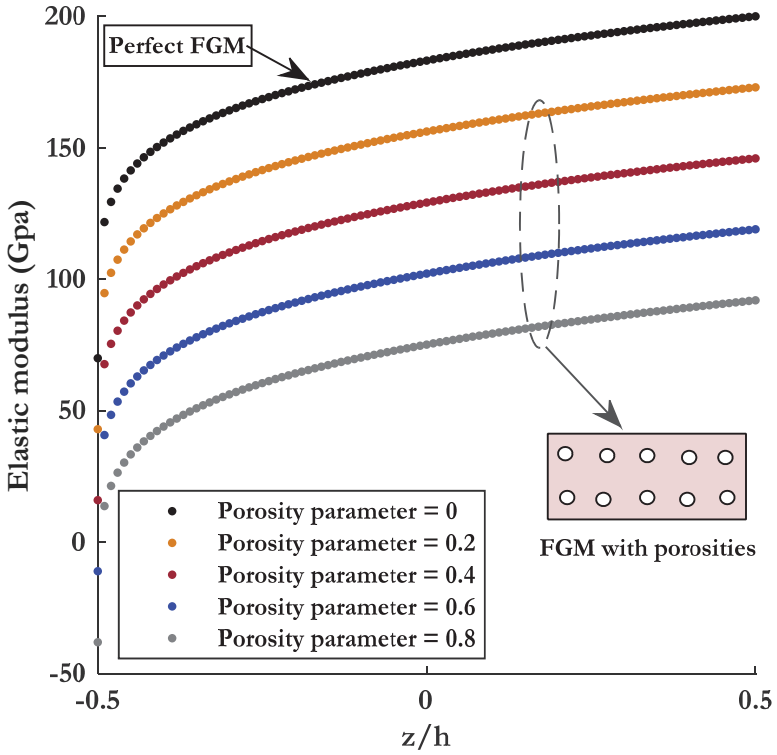

a) Even porosity distribution

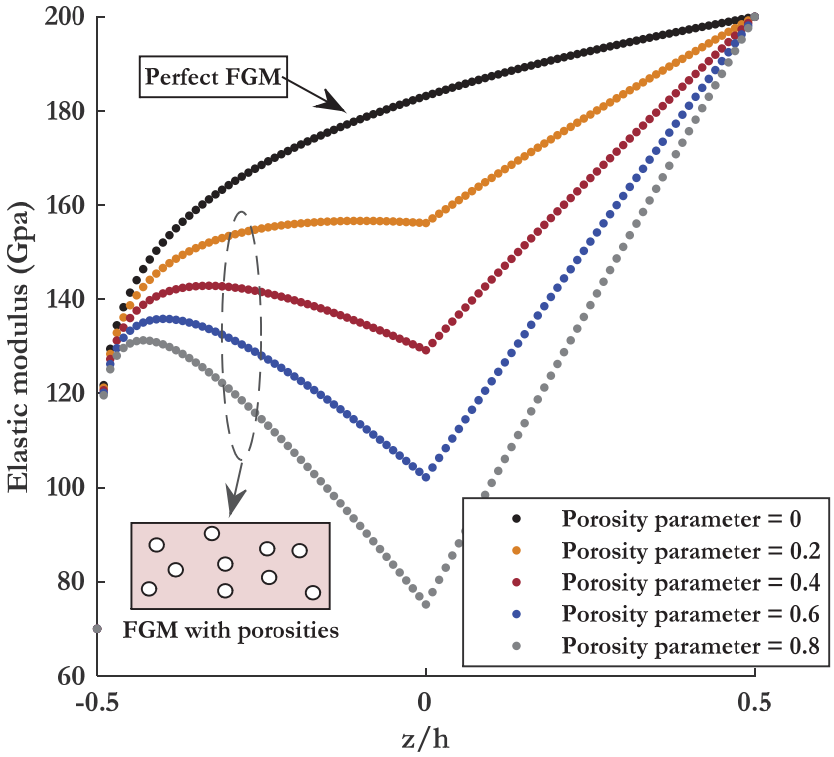

b) Uneven porosity distribution

Figure 5: The effect of the porosity parameter β on the elastic modulus E for two different porosity distributions: a) even porosity and b) uneven porosity.

From the previous Figs. (3–4), the effect of porosities on frequencies is evident, which exposes the structural integrity of the FG plate to the risk of cracking. To enhance our understanding of the effect of porosities on the structural integrity of the FG plate, we study their influence on the mechanical properties (i.e., elastic modulus, mass density, and poisson's ratio). In Fig. 5, the effect of the porosity parameter β on the elastic modulus E of (AL/ZrO_2) FGM at P = 0.2 for two different porosity distributions: a) even porosity and b) uneven porosity. It is clear from Fig. 5a that the elastic modulus reduces when the porosity parameter β varies from 0 to 0.8 (i.e., from perfect FGM to imperfect FGM). For all values of the porosity parameter β, the elastic modulus decreases at the top and bottom surfaces of the plate (purely ceramic and purely metal, $z = \pm h/2$), but the largest decrease occurs at = 0.8, with a difference of 90 Gpa compared to the value of the elastic modulus of the perfect FGM (β = 0). In the case of an uneven porosity distribution (see Fig. 5b), the elastic modulus of imperfect FGM decreases from 70 GPa until it reaches its lowest value at z = 0, then it begins to increase until it reaches 200 GPa. According to the different results obtained in the fourth part, the presence of porosities inside the FG plate leads to a decrease in the mechanical properties and stiffness of the FG plate and thus increases its exposure to cracking and fracture risks. Therefore, developers must devise manufacturing methods that minimize the presence of porosities within the functionally graded materials.

CONCLUSIONS

Currently, plate-type functionally graded materials (FGMs) are widely utilized in various applications and industries. These structural components are subjected to in-plane and dynamic forces, necessitating a structural analysis of FG plates to accurately predict their behavior in bending, buckling, and vibration. Consequently, numerous studies have been conducted on the analysis of FG plates. In this regard, we have undertaken a theoretical investigation focused on analyzing the mechanical behavior of porous FG plates within the elastic framework. The current theory describes the distribution of shear stress utilizing a new hyperbolic function without the need for a shear correction factor, while also satisfying the zero traction boundary conditions on both the top and bottom surfaces of the porous FG plate. The displacement field of the quasi-three dimensional hyperbolic shear deformation theory has six variables including the stretching effect ($\varepsilon_z \neq 0$). The proposed hyperbolic theory is more affluent and presents the transverse shear stress better than third-order, sinusoidal, and exponential shear deformation theories and thus produces better results in describing the mechanical behavior of FG plates. Moreover, the current hyperbolic function does not necessitate a shear correction factor and does not require any adaptation in the event that it is employed as a refined theory. This is due to its form, which is partitioned into two segments, similar to the third-order shear deformation theory. The eigenvalue problem of the provided high-order shear deformation theory is solved using a Navier's solution approach. The influence of power-law index, mode numbers, and geometry on the natural frequencies of porous FG plates is investigated using a comprehensive parametric analysis. Based on the entire results, it is reasonable to conclude:

- The fundamental frequencies obtained by the provided quasi-3D hyperbolic function correspond very well with those obtained by 2D and 3D exact and quasi-3D results in the open literature. Throughout all of the comparison tests, it appears that the present theory provides excellent results for thin, thick, and moderately thick plates.
- The existence of thickness stretching effects ($\varepsilon_z \neq 0$) has led to slight differences between the 2D and quasi-3D results. Therefore, it is necessary to consider this effect to obtain highly accurate outcomes.
- The fundamental frequencies reduce as the power-law indexes (P) and the ratios (a/b) increase, and increase as the ratios (a/h) decrease.
- The presence of porosities within the FG plate reduces its mechanical properties and stiffness, making it more susceptible to cracking and fracture risks. As a result, it is essential to take the presence of porosities into account when analyzing the mechanical behavior of the FG plate.

REFERENCES

[1] Reddy, J. (2000). Analysis of functionally graded plates. International Journal for numerical methods in engineering, 47(1-3), pp. 663-684. DOI: 10.1002/(SICI)1097-0207(20000110/30)47:1/3<663::AID-NME787>3.0.CO;2-8.

[2] Reddy, J. N. and Barbosa, J. I. (2000). On vibration suppression of magnetostrictive beams. Smart Materials and Structures, 9(1), pp. 49. DOI: 10.1088/0964-1726/9/1/305.

[3] Reddy, J. N., Wang, C. M., Lim, G. T. and Ng, K. H. (2001). Bending solutions of Levinson beams and plates in terms of the classical theories. International Journal of Solids and Structures, 38(26-27), pp. 4701-4720. DOI: 10.1016/S0020-7683(00)00298-5.

[4] Zenkour, A. M. (2013). A simple four-unknown refined theory for bending analysis of functionally graded plates. Applied Mathematical Modelling, 37(20-21), pp. 9041-9051. DOI: 10.1016/j.apm.2013.04.022.

[5] Shahsavari, D., Shahsavari, M., Li, L. and Karami, B. (2018). A novel quasi-3D hyperbolic theory for free vibration of FG plates with porosities resting on Winkler/Pasternak/Kerr foundation. Aerospace Science and Technology, 72, pp. 134-149. DOI: 10.1016/j.ast.2017.11.004.

[6] Akavci, S. S. and Tanrikulu, A. H. (2015). Static and free vibration analysis of functionally graded plates based on a new quasi-3D and 2D shear deformation theories. Composites Part B: Engineering, 83, pp. 203-215. DOI: 10.1016/j.compositesb.2015.08.043.

[7] Joshan, Y. S., Santapuri, S. and Grover, N. (2020). Analysis of laminated piezoelectric composite plates using an inverse hyperbolic coupled plate theory. Applied Mathematical Modelling, 82, pp. 359-378. DOI: 10.1016/j.apm.2020.01.050.

[8] Neves, A. M. A., Ferreira, A. J. M., Carrera, E., Cinefra, M., Roque, C. M. C., Jorge, R. M. N. and Soares, C. M. M. (2012). A quasi-3D hyperbolic shear deformation theory for the static and free vibration analysis of functionally graded plates. Composite Structures, 94(5), pp. 1814-1825. DOI: 10.1016/j.compstruct.2011.12.005.

[9] Sarangan, S. and Singh, B. N. (2016). Higher-order closed-form solution for the analysis of laminated composite and sandwich plates based on new shear deformation theories. Composite Structures, 138, pp. 391-403. DOI: 10.1016/j.compstruct.2015.11.049.

[10] Soldatos, K. (1992). A transverse shear deformation theory for homogeneous monoclinic plates. Acta Mechanica, 94(3), pp. 195-220. DOI: 10.1007/BF01176650.

[11] Hebali, H., Tounsi, A., Houari, M. S. A., Bessaim, A. and Bedia, E. A. A. (2014). New quasi-3D hyperbolic shear deformation theory for the static and free vibration analysis of functionally graded plates. Journal of Engineering Mechanics, 140(2), pp. 374-383. DOI: 10.1061/(ASCE)EM.1943-7889.0000665.

[12] Malikan, M. and Eremeyev, V. A. (2020). A new hyperbolic-polynomial higher-order elasticity theory for mechanics of thick FGM beams with imperfection in the material composition. Composite Structures, 249, pp. 112486. DOI: 10.1016/j.compstruct.2020.112486.

[13] Khalfi, Y., BOUCHIKHI, A. S. and BELLEBNA, Y. (2019) "Mechanical Stability Investigation of Advanced Composite Plates Resting on Elastic Foundations Using a New Four-Unknown Refined Theory", Frattura ed Integrità Strutturale, 13(48), pp. 208–221. DOI: 10.3221/IGF-ESIS.48.22.

[14] Touratier, M. (1991). An efficient standard plate theory. International journal of engineering science, 29(8), pp. 901-916. DOI: 10.1016/0020-7225(91)90165-Y.

[15] Mantari, J. L., Oktem, A. S. and Soares, C. G. (2012). A new trigonometric shear deformation theory for isotropic, laminated composite and sandwich plates. International Journal of Solids and Structures, 49(1), pp. 43-53. DOI: 10.1016/j.ijsolstr.2011.09.008.

[16] Neves, A. M. A., Ferreira, A. J. M., Carrera, E., Roque, C. M. C., Cinefra, M., Jorge, R. M. N. and Soares, C. M. M. (2012). A quasi-3D sinusoidal shear deformation theory for the static and free vibration analysis of functionally graded plates. Composites Part B: Engineering, 43(2), pp. 711-725. DOI: 10.1016/j.compositesb.2011.08.009.

[17] Merdaci, S., Hadj Mostefa, A., Beldjelili, Y., Merazi, M., Boutaleb, S. and Hellal, H. (2020) "Analytical solution for statif bending analyses of functionally grades plates with porosities", Frattura ed Integrità Strutturale, 15(55). DOI: 10.3221/IGF-ESIS.55.05.

[18] Chikh, A. (2019) "Investigations in static response and free vibration of a functionally graded beam resting on elastic foundations", Frattura ed Integrità Strutturale, 14(51), pp. 115–126. DOI: 10.3221/IGF-ESIS.51.09.

[19] Karama, M., Afaq, K. S. and Mistou, S. (2009). A new theory for laminated composite plates. Proceedings of the Institution of Mechanical Engineers, Part L: Journal of Materials: Design and Applications, 223(2), pp. 53-62. DOI: 10.1243/14644207JMDA189.

[20] Zaoui, F. Z., Ouinas, D. and Tounsi, A. (2019). New 2D and quasi-3D shear deformation theories for free vibration of functionally graded plates on elastic foundations. Composites Part B: Engineering, 159, pp. 231-247. DOI: 10.1016/j.compositesb.2018.09.051.

[21] Aydogdu, M. (2009). A new shear deformation theory for laminated composite plates. Composite structures, 89(1), pp. 94-101. DOI: 10.1016/j.compstruct.2008.07.008.

[22] Reddy, J. N. (1984). A simple higher-order theory for laminated composite plates. Journal of applied mechanics, pp. 745-752. DOI: 10.1115/1.3167719.

[23] Thai, H. T. and Choi, D. H. (2014). Improved refined plate theory accounting for effect of thickness stretching in functionally graded plates. Composites Part B: Engineering, 56, pp. 705-716. DOI: 10.1016/j.compositesb.2013.09.008.
[24] Merdaci, S. and Mostefa, A. H. (2019) "Influence of porosity on the analysis of sandwich plates FGM using of high order shear-deformation theory"., Frattura ed Integrità Strutturale, 14(51), pp. 199–214. DOI: 10.3221/IGF-ESIS.51.16.
[25] Hebbar, N., Hebbar, I., Ouinas, D. and Bourada, M. (2020) "Numerical modeling of bending, buckling, and vibration of functionally graded beams by using a higher-order shear deformation theory", Frattura ed Integrità Strutturale, 14(52), pp. 230–246. DOI: 10.3221/IGF-ESIS.52.18.
[26] Li, M., Soares, C. G. and Yan, R. (2020). A novel shear deformation theory for static analysis of functionally graded plates. Composite Structures, 250, pp. 112559. DOI: 10.1016/j.compstruct.2020.112559.
[27] Li, M., Soares, C. G. and Yan, R. (2021). Free vibration analysis of FGM plates on Winkler/Pasternak/Kerr foundation by using a simple quasi-3D HSDT. Composite Structures, 264, pp. 113643. DOI: 10.1016/j.compstruct.2021.113643.
[28] Li, M., Yan, R. and Soares, C. G. (2021). Free vibration of advanced composite plates using a new higher order shear deformation theory. European Journal of Mechanics-A/Solids, 88, pp. 104236. DOI: 10.1016/j.euromechsol.2021.104236.
[29] Hadji, M., Bouhadra, A., Mamen, B., Menasria, A., Bousahla, A. A., Bourada, F., ... & Tounsi, A. (2023). Combined influence of porosity and elastic foundation parameters on the bending behavior of advanced sandwich structures. Steel and Composite Structures, 46(1), pp. 1-13. DOI: 10.12989/scs.2023.46.1.001.
[30] Boulefrakh, L., Hebali, H., Chikh, A., Bousahla, A. A., Tounsi, A. and Mahmoud, S. R. (2019). The effect of parameters of visco-Pasternak foundation on the bending and vibration properties of a thick FG plate. Geomechanics and Engineering, 18(2), pp. 161-178. DOI: 10.12989/gae.2019.18.2.161.
[31] Cuong-Le, T., Nguyen, K. D., Nguyen-Trong, N., Khatir, S., Nguyen-Xuan, H. and Abdel-Wahab, M. (2021). A three-dimensional solution for free vibration and buckling of annular plate, conical, cylinder and cylindrical shell of FG porous-cellular materials using IGA. Composite Structures, 259, pp. 113216. DOI: 10.1016/j.compstruct.2020.113216.
[32] Cuong-Le, T., Nguyen, K. D., Hoang-Le, M., Sang-To, T., Phan-Vu, P. and Wahab, M. A. (2022). Nonlocal strain gradient IGA numerical solution for static bending, free vibration and buckling of sigmoid FG sandwich nanoplate. Physica B: Condensed Matter, 631, pp. 413726. DOI: 10.1016/j.physb.2022.413726.
[33] Vu, T. V., Cao, H. L., Truong, G. T. and Kim, C. S. (2022). Buckling analysis of the porous sandwich functionally graded plates resting on Pasternak foundations by Navier solution combined with a new refined quasi-3D hyperbolic shear deformation theory. Mechanics Based Design of Structures and Machines, pp. 1-27. DOI: 10.1080/15397734.2022.2038618.
[34] Vu, T. V., Nguyen-Van, H., Nguyen, C. H., Nguyen, T. P. and Curiel-Sosa, J. L. (2023). Meshfree analysis of functionally graded plates with a novel four-unknown arctangent exponential shear deformation theory. Mechanics Based Design of Structures and Machines, 51(2), pp. 1082-1114. DOI: 10.1080/15397734.2020.1863227.
[35] Vu, T. V., Khosravifard, A., Hematiyan, M. R. and Bui, T. Q. (2019). Enhanced meshfree method with new correlation functions for functionally graded plates using a refined inverse sin shear deformation plate theory. European Journal of Mechanics-A/Solids, 74, pp. 160-175. DOI: 10.1016/j.euromechsol.2018.11.005.
[36] Vu, T. V., Curiel-Sosa, J. L. and Bui, T. Q. (2019). A refined sin hyperbolic shear deformation theory for sandwich FG plates by enhanced meshfree with new correlation function. International Journal of Mechanics and Materials in Design, 15, pp. 647-669. DOI: 10.1007/s10999-018-9430-9.
[37] Vu, T. V., Nguyen, H. T., Nguyen-Van, H., Nguyen, T. P. and Curiel-Sosa, J. L. (2021). A refined quasi-3D logarithmic shear deformation theory-based effective meshfree method for analysis of functionally graded plates resting on the elastic foundation. Engineering Analysis with Boundary Elements, 131, pp. 174-193. DOI: 10.1016/j.enganabound.2021.06.021.
[38] Vu, T. V. (2022). Mechanical behavior analysis of functionally graded porous plates resting on elastic foundations using a simple quasi-3D hyperbolic shear deformation theory-based effective meshfree method. Acta Mechanica, 233(7), pp. 2851-2889. DOI: 10.1007/s00707-022-03242-2.
[39] Kumar, H. N. and Kattimani, S. (2022). Effect of different geometrical non-uniformities on nonlinear vibration of porous functionally graded skew plates: a finite element study. Defence Technology, 18(6), pp. 918-936. DOI: 10.1016/j.dt.2021.05.002.

[40] Ebrahimi, F. and Jafari, A. (2016). A higher-order thermomechanical vibration analysis of temperature-dependent FGM beams with porosities. Journal of Engineering, 2016. DOI: 10.1155/2016/9561504.
[41] Wang, Y. Q. (2018). Electro-mechanical vibration analysis of functionally graded piezoelectric porous plates in the translation state. Acta Astronautica, 143, pp. 263-271. DOI: 10.1016/j.actaastro.2017.12.004.
[42] Fu, T., Wu, X., Xiao, Z. and Chen, Z. (2020). Thermoacoustic response of porous FGM cylindrical shell surround by elastic foundation subjected to nonlinear thermal loading. Thin-Walled Structures, 156, pp. 106996. DOI: 10.1016/j.tws.2020.106996.
[43] Saidi, H. and Sahla, M. (2019). Vibration analysis of functionally graded plates with porosity composed of a mixture of Aluminum (Al) and Alumina (Al2O3) embedded in an elastic medium. Frattura ed Integrità Strutturale, 13(50), pp. 286-299. DOI: 10.3221/IGF-ESIS.50.24.
[44] Thanh, C. L., Tran, L. V., Bui, T. Q., Nguyen, H. X. and Abdel-Wahab, M. (2019). Isogeometric analysis for size-dependent nonlinear thermal stability of porous FG microplates. Composite Structures, 221, pp. 110838. DOI: 10.1016/j.compstruct.2019.04.010.
[45] Srinivas, S., Rao, C. J. and Rao, A. K. (1970). An exact analysis for vibration of simply-supported homogeneous and laminated thick rectangular plates. Journal of sound and vibration, 12(2), pp. 187-199. DOI: 10.1016/0022-460X(70)90089-1.
[46] Mechab, B., Mechab, I. and Benaissa, S. (2012). Analysis of thick orthotropic laminated composite plates based on higher order shear deformation theory by the new function under thermo-mechanical loading. Composites Part B: Engineering, 43(3), pp. 1453-1458. DOI: 10.1016/j.compositesb.2011.11.037.
[47] Hosseini-Hashemi, S., Fadaee, M. O. H. A. M. M. A. D. and Atashipour, S. R. (2011). A new exact analytical approach for free vibration of Reissner–Mindlin functionally graded rectangular plates. International Journal of Mechanical Sciences, 53(1), pp. 11-22. DOI: 10.1016/j.ijmecsci.2010.10.002.
[48] Belabed, Z., Houari, M. S. A., Tounsi, A., Mahmoud, S. R. and Bég, O. A. (2014). An efficient and simple higher order shear and normal deformation theory for functionally graded material (FGM) plates. Composites Part B: Engineering, 60, pp. 274-283. DOI: 10.1016/j.compositesb.2013.12.057.

APPENDIX A

- The stress resultants N, M, S, and Q are defined by:

$$\left(N_x, N_y, N_{xy}\right) = \int_{-h/2}^{h/2} \left(\sigma_x, \sigma_y, \tau_{xy}\right) dz \tag{A1}$$

$$N_z = \int_{-h/2}^{h/2} g'(z)\sigma_z \, dz \tag{A2}$$

$$\left(M_x, M_y, M_{xy}\right) = \int_{-h/2}^{h/2} \left(\sigma_x, \sigma_y, \tau_{xy}\right) z \, dz \tag{A3}$$

$$\left(S_x, S_y, S_{xy}\right) = \int_{-h/2}^{h/2} \left(\sigma_x, \sigma_y, \tau_{xy}\right) f(z) \, dz \tag{A4}$$

$$\left(Q_{xz}, Q_{yz}\right) = \int_{-h/2}^{h/2} \left(\tau_{xz}, \tau_{yz}\right) g(z) \, dz \tag{A5}$$

- The moments of inertia (D_{ij}) are defined as:

$$D_i = \int_{-h/2}^{h/2} \rho(z)\left(1, z, z^2, f(z), z f(z), (f(z))^2, g(z), (g(z))^2\right) dz \qquad i = 1,8 \tag{A6}$$

APPENDIX B

- The stiffness coefficients ($A_{ij}, B_{ij}, V_{ij}, D_{ij}, E_{ij}, F_{ij}, G_{ij}, K_{ij}, L_{ij}$) can be determined as below:

$$\left(A_{11}, A_{12}, A_{22}, A_{33}\right) = \int_{-h/2}^{h/2} \left(C_{11}, C_{12}, C_{22}, C_{44}\right) dz \tag{B1}$$

$$\left(B_{11}, B_{12}, B_{22}, B_{33}\right) = \int_{-h/2}^{h/2} \left(C_{11}, C_{12}, C_{22}, C_{44}\right) z\, dz \tag{B2}$$

$$\left(E_{11}, E_{12}, E_{22}, E_{33}\right) = \int_{-h/2}^{h/2} \left(C_{11}, C_{12}, C_{22}, C_{44}\right) z^2\, dz \tag{B3}$$

$$\left(V_{11}, V_{12}, V_{22}, V_{33}\right) = \int_{-h/2}^{h/2} \left(C_{11}, C_{12}, C_{22}, C_{44}\right) f(z)\, dz \tag{B4}$$

$$\left(F_{11}, F_{12}, F_{22}, F_{33}\right) = \int_{-h/2}^{h/2} \left(C_{11}, C_{12}, C_{22}, C_{44}\right) z\, f(z)\, dz \tag{B5}$$

$$\left(H_{11}, H_{12}, H_{22}, H_{33}\right) = \int_{-h/2}^{h/2} \left(C_{11}, C_{12}, C_{22}, C_{44}\right) (f(z))^2\, dz \tag{B6}$$

$$\left(D_{11}, D_{12}\right) = \int_{-h/2}^{h/2} \left(C_{12}\right) g'(z)\, dz \;\; ; \;\; \left(G_{11}, G_{12}\right) = \int_{-h/2}^{h/2} \left(C_{12}\right) z\, g'(z)\, dz \tag{B7}$$

$$\left(K_{11}, K_{12}\right) = \int_{-h/2}^{h/2} \left(C_{12}\right) f(z)\, g'(z)\, dz \tag{B8}$$

$$\left(M_{44}, M_{55}\right) = \int_{-h/2}^{h/2} \left(C_{55}\right) (g(z))^2\, dz \;\; ; \;\; L_{11} = \int_{-h/2}^{h/2} \left(C_{11}\right) g'(z)\, g'(z) dz \tag{B9}$$